Accepted Manuscript

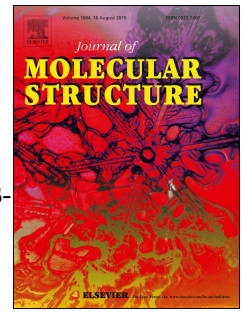

Synthesis, structural characterization, and theoretical studies of new pyrazole (*E*)-2-{[(5-(*tert*-butyl)-1*H*-pyrazol-3-yl)imino]methyl}phenol and (*E*)-2-{[(1-(4-bromophenyl)-3-(*tert*-butyl)-1*H*-pyrazol-5-yl]imino]methyl}phenol

Fernando Cuenú, Andrés Restrepo-Acevedo, María Isabel-Murillo, John Eduard Torres, Rodolfo Moreno-Fuquen, Rodrigo Abonia, Alan R. Kennedy, Juan Carlos Tenorio, Christian W. Lehmann

PII: S0022-2860(19)30128-0

DOI: https://doi.org/10.1016/j.molstruc.2019.02.004

Reference: MOLSTR 26161

To appear in: *Journal of Molecular Structure*

Received Date: 30 December 2018

Revised Date: 2 February 2019

Accepted Date: 3 February 2019

Please cite this article as: F. Cuenú, André. Restrepo-Acevedo, Marí. Isabel-Murillo, J. Eduard Torres, R. Moreno-Fuquen, R. Abonia, A.R. Kennedy, J.C. Tenorio, C.W. Lehmann, Synthesis, structural characterization, and theoretical studies of new pyrazole (*E*)-2-{[(5-(*tert*-butyl)-1*H*-pyrazol-3-yl)imino]methyl}phenol and (*E*)-2-{[(1-(4-bromophenyl)-3-(*tert*-butyl)-1*H*-pyrazol-5-yl]imino]methyl}phenol, *Journal of Molecular Structure* (2019), doi: https://doi.org/10.1016/j.molstruc.2019.02.004.

GRAPHICAL ABSTRACT

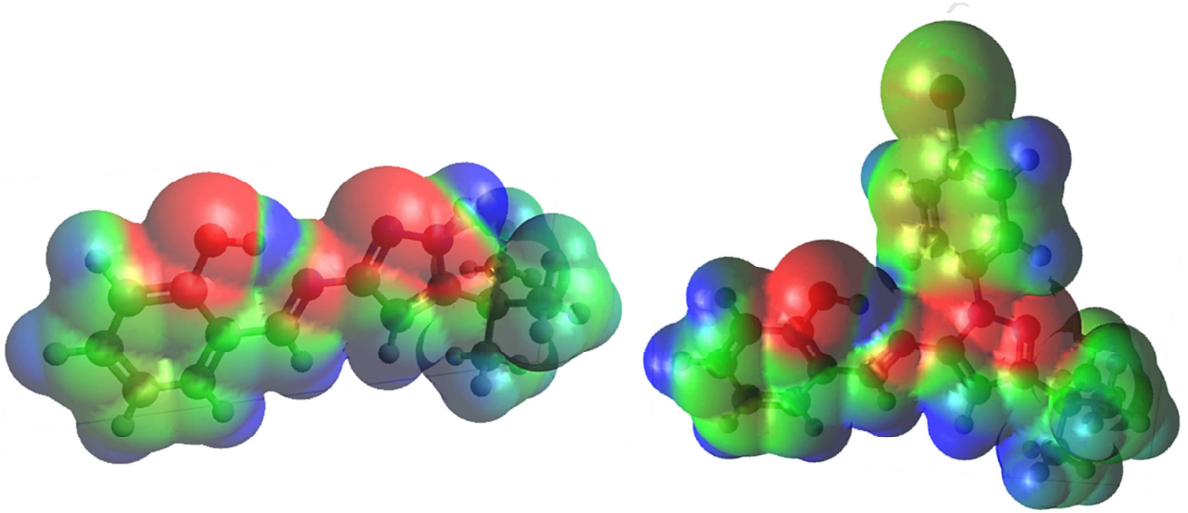

Synthesis, structural characterization, and theoretical studies of new pyrazole (*E*)-2-{[(5-(*tert*-butyl)-1*H*-pyrazol-3-yl)imino]methyl}phenol and (*E*)-2-{[(1-(4-bromophenyl)-3-(*tert*-butyl)-1*H*-pyrazol-5-yl]imino]methyl}phenol

Fernando Cuenú [a,*], Andrés Restrepo-Acevedo [a], María Isabel-Murillo [a], John Eduard Torres [a], Rodolfo Moreno-Fuquen [b], Rodrigo Abonia [b], Alan R. Kennedy [c], Juan Carlos Tenorio [d], Christian W. Lehmann [d]

[a]Laboratory of Inorganic Chemistry and Catalysis, Chemistry Program, Universidad del Quindío, Carrera 15, Calle 12 Norte, Armenia-Colombia
[b]Department of Chemistry, Universidad del Valle, Calle 13 No. 100-00, A.A. 25360, Cali-Colombia
[c]Department of Pure & Applied Chemistry. University of Strathclyde, 295 Cathedral Street, Glasgow G1 1XL Scotland
[d]Max-Planck-Institut für Kohlenforshung, Kaiser-Wilhelm-Platz 145470 Mülheim an der Ruhr, Germany

***Corresponding Author:** Laboratory of Inorganic Chemistry and Catalysis, Chemistry Program, Universidad del Quindío, Carrera 15, Calle 12 Norte, Armenia-Colombia. Mail: fercuenu@uniquindio.edu.co

ABSTRACT

In this paper, theoretical and experimental studies of two new Schiff bases were performed. The (*E*)-2-{[(5-(*tert*-butyl)-1*H*-pyrazol-3-yl)imino]methyl}phenol (**3**) and (*E*)-2-{[(1-(4-bromophenyl)-3-(*tert*-butyl)-1*H*-pyrazol-5-yl]imino]methyl}phenol (**5**) compounds were characterized by spectroscopic techniques, (i.e. MS, NMR, FT-IR, UV-vis, and single-crystal X-ray diffraction). The molecular geometry of both compounds in the ground state, vibrational frequencies, and chemical shift were calculated by using the functional density theory method, with B3LYP as functional and 6-31G** as basis set, using the GAUSSIAN 09 program package. With the VEDA 4 program, the vibrational frequencies were allocated in terms of potential energy distribution (PED). In this paper, theoretical and experimental studies of two new Schiff bases were performed. The (*E*)-2-{[(5-(*tert*-butyl)-1*H*-pyrazol-3-yl)imino]methyl}phenol (**3**) and (*E*)-2-{[(1-(4-bromophenyl)-3-(*tert*-butyl)-1*H*-pyrazol-5-yl]imino]methyl}phenol (**5**) compounds were characterized by spectroscopic techniques, (i.e. MS, NMR, FT-IR, UV-vis, and single-crystal X-ray diffraction). The molecular geometry of both compounds in the ground state, vibrational frequencies, and chemical shift were calculated by using the functional density theory method, with B3LYP as functional and 6-

31G** as basis set, using the GAUSSIAN 09 program package. With the VEDA 4 program, the vibrational frequencies were allocated in terms of potential energy distribution (PED). Molecular stabilities were determined in terms of softness and hardness, and the values were determined from the energies of HOMO and LUMO orbitals. Remarkably, good agreements between the calculated IR, NMR and UV-vis spectra in comparison to those experimental ones, were found.

KEYWORDS: Pyrazoles, Schiff bases, FT-IR, NMR, Electronic absorption spectra, DFT.

1. INTRODUCTION

Nitrogen containing heterocyclic rings, are the main frameworks of various biologically active compounds showing a vast variety of applications in pharmacological and agrochemical industries. Because of their widespread potential of pharmacological activities, such as anti-inflammatory [1], antitumor [2], anticonvulsant [3], and antimicrobial [4], the pyrazole ring and its derivatives are recognized in the literature as important biologically active heterocyclic compounds. Additionally, many pyrazole derivatives have also been used in catalysis, functional coordination ligands, and organic light emitting diodes [5-8].

Schiff bases containing azomethine bonds (-N=C-) are usually formed via the condensation reaction of a primary amine with an aldehyde or ketone mediated by straightforward protocols without stringent reaction conditions and water as only by-product [9]. Substituted Schiff bases with π-conjugation play a vital role in the development of new generation of electronic and photonic devices due to delocalization of electrons [10].

This study describes the synthesis, characterization, and computational calculations of two new Schiff bases, (*E*)-2-{[(5-(*tert*-butyl)-1*H*-pyrazol-3-yl)imino]methyl}phenol (**3**) and (*E*)-2-{[(1-(4-bromophenyl)-3-(*tert*-butyl)-1*H*-pyrazol-5-yl]imino]methyl}phenol (**5**), with the purpose of studying structural properties by using the functional density theory (DFT) together with B3LYP and the standard set of bases 6-31G**. In addition, calculations of the vibrational frequencies of the optimized geometries were performed to explain the differences

between the solid and gaseous phases of the studied compounds. The chemical shifts in their ^{1}H and ^{13}C NMR spectra were calculated, as well as, the energy of the molecules to determine the highest occupied molecular orbitals and lowest unoccupied molecular orbitals (HOMO-LUMO, respectively) in order to calculate their UV-vis spectra. Our research group has been interested in synthesizing aminopyrazoles [11], to be used in the formation of imino-pyrazoles (i.e. Schiff bases) of biological and physicochemical interest. In our previous investigations, computational studies of the Schiff base {(*E*)-[(3-*tert*-butyl-1-phenyl-1*H*-pyrazol-5-yl)imino]methyl}phenol [12] were performed. Now, in this work, we wish to compare and discuss some physicochemical properties, like hardness, softness, and electronegativity between two new synthesized Schiff bases.

2. Experimental

2.1. Analytical and physicochemical measurements

All chemicals and solvents used (analytical grade), were purchased from Sigma-Aldrich and Across, and used without further purification. The reactions were monitored by thin layer chromatography (TLC) using silica gel 60 F_{254} (Merck) alumina plates. The melting points were determined on a Büchi melting point apparatus. Infrared spectra were taken on a Perkin Elmer FT 2000 series spectrophotometer using KBr disks. The NMR spectra were recorded on a Bruker Advance 400 spectrophotometer operating at 400 MHz for ^{1}H and at 100 MHz for ^{13}C, using DMSO-d_6 as solvent and tetramethylsilane as internal standard. Chemical shifts (δ) are in ppm and the coupling constants (J) are in Hertz (Hz). The mass spectra were obtained on a SHIMADZU-GCMS 2010-DI-2010 spectrometer equipped with a direct input probe operating at 70 eV. The UV-Vis absorption spectra were obtained in a range of 200-600 nm using a Shimadzu UV-Vis 160 spectrophotometer. Microanalyses were performed on an Agilent CHNS elemental analyzer.

2.2. Synthesis

2.2.1. Synthesis of aminopyrazole

2.2.1.1. The 5-(*tert*-butyl)-1*H*-pyrazole-3-amine (**1)** was obtained following a previously reported procedure [13]. Thus, in a test tube, a mixture of 4,4-dimethyl-oxopentanenitrile (1.0 g, 7.9 mmol) and hydrazine monohydrate (0.443 g, 8.66 mmol) was placed. The solvent-free mixture was heated at 130 °C until complete consumption of the starting materials, affording a white solid in 98% yield. No further purification was required.

2.2.1.2 The 1-(4-bromophenyl)-3-(*tert*-butyl)-1*H*-pyrazol-5-amine (**4**), was prepared, as described in the literature [14]. To a concentrated hydrochloric acid solution (3.8 mL) in water (33 mL) was added (4-bromophenyl)hydrazine (2.12 g, 11.41 mmol) and 4,4-dimethyl-3-oxopentanenitrile (1.85 g, 14.79 mmol). The mixture was heated at 70 °C for 1 h, then, additional concentrated hydrochloric acid (3.8 mL) was added and the mixture was heated for one additional hour. After cooling, crushed ice was added and the mixture was neutralized with concentrated ammonium hydroxide. The resulting solid was filtered under reduced pressure, washed with cold water (3×5 mL). The starting precursor **2** was obtained in 86% yield as a light brown solid. No further purification was required.

*2.2.2. Synthesis of the compounds **3** and **5***

A mixture of the aminopyrazole (**1** or **4**) (1.44 mmol), 2-hydroxybenzaldehyde (**2**) (1.44 mmol) and glacial acetic acid (5 drops) was stirred for 10 min at room temperature. After the reaction was complete (monitored by TLC), the crude solid formed was washed with cold water (5 × 20 mL) and filtered under vacuum to dryness, affording the compounds **3** as a yellow solid in 96% yield and **5** as a beige solid in 97% yield. Single-crystals of compounds **3** and **5**, suitable for X-ray diffraction (XRD), were grown by slow evaporation of a CH_2Cl_2 solution at room temperature. The synthetic procedures for compounds **3** and **5** are shown in **Scheme 1** and **Scheme 2**, respectively.

Insert Scheme 1.

Insert Scheme 2.

*(E)-2-{[(5-(tert-Butyl)-1H-pyrazol-3-yl)imino]methy}phenol (**3**)*

Anal. Cal. for $C_{14}H_{17}N_3O$: %C 69.11, %H 7.04, %N 17.25. Found: %C 69.22, %H 7.08, %N 17.31. M.p. 197-199 °C. MS (70 eV) *m/z* (%) 243 [M^+] (100), 226 [M^+-17] (92.33), 228 [M^+ -15] (14.75), 186 [M^+ -57] (1.40) (see Supp. Inf. S1, S2). IR (KBr, cm^{-1}) νN-H 3140

(pyrazole), ν C-H 3085 (pyrazole), ν_{as} –CH_3 2957, ν_s –CH_3 2857, ν –C=N 1607. ^{1}H NMR (400 MHz, DMSO-d_6, δ in ppm) 1.31 (s, 9H, *t*Bu-H); 6.33 (s, 1H, H-9); 6.97 (m, 2H, H-3 and H-5); 7.40 (t, 1H, ^3J = 7.49 Hz, H-4); 7.62 (d, 1H, ^3J =7.61 Hz, H-6); 9.07 (s, 1H, H-7); 12.61 (bs, 1H, OH); 13.23 (bs, 1H, NH). ^{13}C NMR (100 MHz, DMSO-d_6, δ in ppm) 30.3 (*t*BuC); 31.3 (C-11); 92.2 (C-9); 117.0 (C-3); 119.6 (C-5); 119.8 (C-8); 132.7 (C-6); 133.3 (C-4); 154.7 (C-10); 156.0 (C-1); 160.7 (C-2); 162.4 (C-7). The atoms were numbered according to **Figure 1 (compound 3)**. UV-Vis in MeCN, λ max nm, (log ε): λ_1 194 (4.42), λ_2 217 (4.36), λ_3 231 (4.19), λ_4 281 (4.22), λ_5 307 (4.23), λ_6 338 (4.26).

*(E)-2-{[(1-(4-Bromophenyl)-3-(tert-butyl)-1H-pyrazol-5-yl]imino]methyl}phenol (**5**)*

Anal. Cal. for $C_{20}H_{20}N_3OBr$: %C 60.31, %H 5.06, %N 10.55. Found: %C 60.18, %H 5.11, %N 10.68%. M.p: 140-142 °C. MS: (70 eV) *m/z* (%) 399 (*M+2*, 98), 397 (M^+, 100), 384 (M^+-15, 60), 382 (M^+-15, 81), 359 (24), 357 (26) (see Supp. Inf. S3, S4). IR (KBr, cm^{-1}) ν C-H 3119 (pyrazole), ν C-H 3054 (aromatic), ν_{as} –CH_3 2955, ν_s –CH_3 2861, ν-C=N 1604, ν-C-Br 749. ^{1}H NMR (400 MHz, DMSO-d_6, δ in ppm) 1.34 (s, 9H *t*Bu-H); 6.70 (s, 1H, H-9); 6.95 (d, 1H, ^3J = 8.3 Hz, H-3); 7.00 (t, 1H, ^3J = 7.5 Hz, H-5); 7.45 (t, 1H, ^3J = 8.0 Hz, H-4); 7.63 (d, 2H, *J* = 8.8 Hz, H-16); 7.69 (d, 1H, *J* = 1.6 Hz, H-6); 7.74 (d, 2H, *J* = 8.81 Hz, H-17); 9.13 (s, 1H, H-7); 11.60 (bs, 1H, OH); ^{13}C NMR (100 MHz, DMSO-d_6, δ in ppm) 30.6 (*t*BuC); 32.7 (C-11); 92.0 (C-9); 117.2 (C-3); 120.1 (C-5); 120.2 (C-15); 120.3 (C-1); 126.5 (C-16); 132.0 (C-6); 132.4 (C-17); 134.5 (C-4); 138.6 (C-18); 149.0 (C-8); 160.1 (C-2); 162.5 (C-10); 163.0 (C-7). The atoms were numbered according to **Figure 1 (compound 5)**. UV-Vis in MeCN, λ max nm, (log ε): λ_1 195 (4.79), λ_2 205 (4.92), λ_3 236 (4.62), λ_4 280 (4.21), λ_5 311 (4.23), λ_6 325 (4.34), λ_7 360 (4.3).

2.3. X-ray crystal structure determination

Crystal data for compounds **3** and **5** were deposited at CCDC with the reference number CCD 1884085 and 1883927 respectively.

Insert Table 1.

3. Computational study

Theoretical calculations were determined in the gas phase and in the approximation of the isolated molecule. Molecular optimization, harmonic vibration frequencies, and energy values were calculated by using the DFT computational method, incorporating the Beck's three-parameter exchange coupled with B3LYP correlation functional density hybrid with the base set 6-31G** and the Gaussian packet 09 [15] without any obstacle to geometry. Nuclear magnetic resonance calculations were carried out to quantify the chemical shifts of protons with the gauge-independent atomic orbital (GIAO) method.

The molecular visualization software was used for the vibration frequencies where they were analyzed in terms of potential energy distribution (PED), using the VEDA 4 program [16], and the contribution percentage of the border orbitals in each transition of the electron absorption spectra was performed by using The GaussSum program [17]. The frequencies and bond lengths found in DFT methods provided good results compared to the experimental values.

4. Results and Discussion

4.1. Structural analysis

Table 2 shows that the parameters of the optimized structures of compounds **3** and **5** calculated by the DFT/B3LYP method agree well with experimental data obtained through XRD. The numbering of the atoms is given in **Figure 2.** The relation between calculation and experimental data was obtained by linear function formula (see supplementary data, Figure S5).

Insert Table 2.

For most bond distances and bond angles, the calculated values were very close to the experimental ones and did not present significant deviations, as observed in **Table 2**. Significant differences were observed in O-H and N-H bonds, which are associated with fact that, in the solid state the experimental results are related to molecular packing, where hydrogen bonds are relevant, while isolated molecules in gas phase are considered for theoretical calculations (i.e. no hydrogen bonds are present). Moreover, in the solid state, it is

observed that the presence of a crystal field together with the intermolecular interactions connects the molecules together, giving rise to the variance in the binding parameters between the calculated and experimental values [18].

Insert Figure 1.

Insert Figure 2.

4.2 Supramolecular features

The projection of the molecular structure, generally related to atoms and covalent bonds, towards a level dominated by non-covalent interactions should lead to the use of new rules governing these structures, their dynamics, transformations and properties of molecular assemblies. It is therefore interesting to undertake a supramolecular study of compounds **3** and **5** to find the non-covalent relationships governing each molecular structure[19].

*4.2.1 Compound **3***

The relatively high directionality and strength of hydrogen bonds can predict, in certain organic compounds, their orientation and behavior during the crystalline growth process. This system has intra-intermolecular hydrogen bonds in its crystalline growth. An intramolecular, relatively strong, O1-H1...N1 hydrogen bond [20] is observed and this allows to approximately maintaining the planarity of the phenol ring with the central segment as shown in **Figure 3**.

A relatively strong intermolecular hydrogen bond N3-H1H...N2 is observed. The N3 atom in the molecule at (x,y,z) acts as hydrogen bond donor to the N2 atom of the pyrazole ring in the molecule at (y+1/4,-x+3/4,-z+7/4). At the same time, two relatively weak intermolecular hydrogen bonds are observed. The C7-H7 and C9-H9 groups in the molecule at (x,y,z) act as hydrogen bond donors to the O1 atom in the molecule at (-y+1/4,+x-1/4,+z-1/4) (**Table 3**). These interactions permitted to observe an arrangement with a fascinating architecture, involving the formation of R^{15}_{14} (81) synthons, facilitating crystalline system growth in the b direction (**see Figure 3**).

Insert Figure 3.

The central segment C1-C7-N1-C8 forms a dihedral angle with the phenol ring of 2.83 (10)^{o} and with the pyrazole ring of 5.78 (12)^{o}.

*4.2.2 Compound **5***

This system has a relatively strong intramolecular O1-H1H ... N1 hydrogen bond, similar to the intramolecular bond presented in the compound **3** system, which enables observing a planarity between the phenol ring and the central C1-C7-N1-C8 segment. Additionally, a relatively weak C7-H7...N3 bond is observed. The C7-H7 group in the molecule at (x,y,z) acts as hydrogen bond donor to the N3 atom of the pyrazole ring in the molecule at (x,-y+3/2,z+1/2) as shown in **Figure 4** (**Table 3**). The central segment forms dihedral angles with the phenol and pyrazole ring of 4.36 (15)^{o} and 12.75 (16)^{o}, respectively. This segment, additionally, forms a dihedral angle of 58.44 (6)^{o} with the bromophenol ring (**see Figure 4** and **Table 3**).

Insert Figure 4.

4.3 Vibrational assignments

Table 4 lists the wave numbers of the bands observed in the FT-IR spectra of the compounds **3** and **5**. The theoretical frequencies and infrared intensities were calculated by the DFT/B3LYP method.

Insert Table 4.

The experimental vibrational FT-IR spectra for **3** and **5** (**Figure 5**) shows the vibration frequencies due to asymmetric -CH_3 stretching at 2964 cm^{-1} and symmetrical -CH_3 stretching at 2861 cm^{-1}, corresponding to *tert*-butyl group for compound **3**. For compound **5** it is observed the -CH_3 stretching at 2958 cm^{-1} and symmetrical -CH_3 stretching at 2861 cm^{-1}. Stretching of the imine group -C=N is observed at 1614 and 1604 cm^{-1} for compounds **3** and **5**, respectively. The N-H absorption band of compound **3** is observed at 3143 cm^{-1}. The

characteristic band of the hydroxyl group does not appear in the IR of both compounds; this finding could be attributed to the formation of intramolecular hydrogen bonding between the nitrogen atom of the imine (N1) and the hydrogen of the hydroxyl (O1-H) group.

Comparison of the calculated frequencies, B3LYP with the experimental values, reveals overestimation of the vibration modes calculated due to the neglect of the harmonicity in the real system. Correction of the methods was performed according to Cruz *et al*. [21], Scale factor for the described method (DFT-B3LYP/6-31G**) was 0.960461 . For the assignment of frequencies, the VEDA 4 program was used.

Figure 5 shows the calculated (with DFT) and experimental spectra for compounds **3**.and **5**. **Figure S6** (see supplementary data), shows correlation curves between the calculated and experimental data, where correlation coefficients (R^2) = 0.9993 for **3**, and (R^2) = 0.9988 for **5** indicates that the results of the theoretical method provide an excellent fit to the experimental values.

Insert Figure 5.

4.3.1. N-H Stretching

The N-H stretching band usually appears in the 3220-3100 cm^{-1} region [22]. In the experimental IR spectrum of compound **3** this absorption band was observed at 3143 cm^{-1}. This vibration was also calculated by B3LYP obtaining a value of 3530 cm^{-1}. These results are consistent with those reported in the literature by Tanis *et al.,* [23].

4.3.2. O-H and C-OH vibrations

It has been shown that the frequency of the absorption vibration of the O-H group in the gas phase is approximately 3657 cm^{-1} [24-25]. The vibration of the OH functionality was not observed in the experimental spectra of compounds **3** and **5** due to a widening of the band [24], attributed to aforementioned intramolecular hydrogen bond. The calculated values for **3** and **5** are shown at 3029 and 3161 cm^{-1}, respectively. The difference appears as a result of the theoretically calculated values that do not consider the Coulombian attraction generated by

the imino-nitrogen atom over the phenolic hydrogen that avoids vibration of the bond, which is consistent with a strong intramolecular hydrogen bond reported by Harold *et al.*, [26]. Binil *et al.*, [27] reported the vibration of the C-OH bond for [4-butyl-1-(4-hydroxyphenyl)-2-phenyl-3,5-pyrazolydinedione] at 1211 cm^{-1}; in this study this vibration is observed in the experimental IR spectra of **3** and **5** at 1213 and 1283 cm^{-1}, respectively, agreeing with that reported by us recently [28].

4.3.3. Aromatic stretching

An aromatic moiety usually is recognized in IR by the presence of C-H vibration-stretching in the 3100-3000 cm^{-1} [29] region and these vibrations are not generally affected by the ring substitution [29]. In our study, the experimental frequency of C-H stretching appears at 3091 cm^{-1} for compound **3** and at 3058 cm^{-1} for compound **5**. These frequencies matches with the calculated values at 3089 cm^{-1} for **3** and 3081 cm^{-1} for **5**.

4.3.4. tert-Butyl C-H stretching

The stretching vibration of aliphatic C-H bonds appear below 3000 cm^{-1} [30]. The theoretical spectra show these vibrations at 3003 and 2926 cm^{-1} for compound **3** and at 2983 and 2963 cm^{-1} for compound **5**. These signals are related to the asymmetric and symmetrical sp^3 (CH) vibrations. The C-H stretching frequencies of the *tert*-butyl group in the experimental spectra were observed at 2964 and 2861 cm^{-1} for compound **3** and at 2958 and 2861 cm^{-1} for compound **5**.

4.3.5. C-C Stretching

The C=C vibrations of the aromatic ring are generally found in the region of 1650 and 1400 cm^{-1} [31]. These absorptions bands are observed at 1571 and 1567 cm^{-1} in the experimental spectra of both compounds while the calculated values appear at 1550 and 1540 cm^{-1} for compound **3** and **5** respectively.

4.3.6. C=N and C-N Vibrations

The strong bands appearing in the region of 1614 and 1604 cm^{-1} in the experimental spectra of compounds **3** and **5**, respectively, are attributed to their C=N bonds, which are characteristic absorption bands of Schiff-base derivatives [32]. These bands appear in the theoretical spectra at 1611 cm^{-1} for compound **3** and at 1598 cm^{-1} for compound **5**.

In general, identification of the C-N vibration is a difficult task, given that in this region (i.e. 1600-1000 cm^{-1}) [33], it can be mixed with other bands (fingerprints region); however, C-N stretching assignments are identified by the application of the GaussView graphical interface [34]. The C-N stretching absorbs in the range of 1382-1266 cm^{-1} [35]; in the experimental spectra, this band appeared at 1279 cm^{-1} for compound **3** and at 1381 cm^{-1} for compound **5**. In the theoretical spectra the same bands appear at 1405 cm^{-1} and 1433 cm^{-1}, respectively.

4.4. NMR studies

The nuclear magnetic resonance (NMR) spectrum is frequently used to analyze each H and C atom in different chemical environments of the target compound [36]. DFT Theory level optimization with the base 6-31G** and GIAO method were used to calculate the chemical shifts of ^{1}H and ^{13}C NMR [37], of compounds **3** and **5**.

The experimental and theoretical chemical shifts of ^{1}H and ^{13}C in DMSO-d_6 as solvent are shown in **Table 5**, (the atoms were numbered according to **Figure 2**). The experimental ^{1}H and ^{13}C spectra of the studied molecules **3** and **5** are shown in Supp. Inf. S7, S8 for compound **3** and Supp. Inf. S9, S10 for **5**, respectively.

Insert Table 5.

4.4.1. ^{1}H NMR

The experimental ^{1}H NMR spectra have good correlation with the theoretical ^{1}H NMR. The correlation coefficient (R^2) found for ^{1}H NMR chemical shifts was 0.9983 for compound **3** and 0.9966 for compound **5** (Supp. Inf. S11). In the experimental ^{1}H NMR spectra of compounds **3** and **5** appears 8 and 9 signals that integrate for seventeen and twenty protons, respectively.

Usually the chemical shifts of aromatic protons in organic molecules are observed in the range of 7.00-8.00 ppm. In the experimental ^{1}H NMR spectra, chemical shifts of aromatic protons appears in the range 6.95-7.61 ppm for compound **3** and 6.95-7.73 ppm for **5** while, the calculated ^{1}H NMR afforded chemical shifts in the range of 7.07-7.64 ppm for compound **3** and 7.08-8.06 ppm for **5**. Thus, both experimental and calculated values agree with the expected common chemical shifts range (i.e. 7.00-8.00 ppm).

The azomethyne protons appear at 9.07 and 9.12 ppm in the experimental spectra of compounds **3** and **5**, respectively, which is consistent with this type of protons in Schiff bases (HC=N) [40-41]. These signals are observed in the theoretical spectra at 8.94 and 8.90 ppm for compounds **3** and **5** respectively, in a very good agreement between both studies. At 13.23 and 11.61 ppm appears broad singlets in the experimental spectra of compounds **3** and **5**, respectively, assigned to protons of the -OH functionality. In the theoretical spectra these signals appears at 13.45 and 12.45 ppm, respectively. Particularly, in compound **5** there is a good correlation between the experimental and theoretical values. However, an appreciable discrepancy is observed in compound **3**, the N-H proton appear at 12.61 ppm in the experimental and 9.42 ppm in theoretical NMR**.** This finding could be associated with a major solvent effect (i.e. the polar DMSO) in compound **3** compared with compound 5 due the presence of two protic N-H and O-H hydrogen atoms.

4.4.2. ^{13}C NMR

Taking into account that the ^{13}C NMR chemical shifts interval for analogous aromatic organic molecules is usually >100 ppm [38-39], the accuracy between calculated and experimental spectra ensures reliable interpretation of spectroscopic parameters [38]. In consequence, our (R^2) of calculated ^{13}C NMR chemical shifts was 0.9991 for compound **3** and 0.9907 for compound **5** (Supp. Inf. S12). Twelve signals for fourteen carbon atoms and sixteen signals for twenty carbon atoms are observed in the experimental ^{13}C NMR spectra for compounds **3** and **5** respectively. The aromatic carbons give signals in the overlapped areas of the spectrum with chemical shift values from 100 to 150 ppm [42]; Similarly, chemical shifts were observed in the values calculated between 102 to 147 ppm for compound **3** and 102 to 148 for compound **5**, while the chemical shifts in the experimental values were observed between 117

to 160 ppm for compound **3** and 117 to 162 ppm for compound **5**. The carbon atom signal of the azomethine functionality is observed at 162.43 and 162.49 ppm in the experimental spectra of compounds **3** and **5**, respectively, consistent with that reported in the literature [37], whereas the theoretical calculations showed these signals at 145.80 and 147.73 ppm.

In general, the experimental results of ^{1}H and ^{13}C NMR with the level DFT/6-31G** represent a good approximation to the data observed experimentally.

4.5. Electronic properties

The electronic absorption spectra of compounds **3** and **5** were measured in acetonitrile solution and were compared with the calculated spectra at time dependent DFT (TD-DFT) calculations based on the optimized molecular structure, as shown in **Figure 6**.

The theoretical calculations for compound **3** predicts an electronic transition of 3.699 eV with an oscillator strength of f = 0.480 at 335 nm, showing good agreement with the measured experimental data (338 nm) is assigned to the π→π* transition within the -C=N azomethine group [43-46]. The calculations also predicted electronic transitions at 291 nm (4.260 eV), which is equivalent to experimental absorption band at 293 nm. In compound **5** the theoretical calculations predicted an electronic transition of 3.399 eV with an oscillator strength of f = 0.496 at 364 nm, showing good agreement with the measured experimental data (360 nm) is assigned to the π→π* transition within the -C=N azomethine group [43-46].

Insert Figure 6.

In the UV–Vis spectra of compounds **3** and **5**, The remaining three absorption bands at 193/195, 216/205, and 231/236 nm for compounds **3**/**5**, respectively, are assigned to π→π * transitions associated to the aromatic rings (pyrazole and OH-phenyl) [28].

Insert Table 5.

4.6. Molecular electrostatic potential (MEP)

The molecular electrostatic potential (MEP) was investigated through DFT-B3LYP theoretical calculations at the 6-31G** level. The MEP mapping is very useful in the

investigation of the molecular structures with their physicochemical property relationships [47–50]. The color scheme for the MEP surface is: red (partially negative charge or electron rich); blue (partially positive charge or electron deficient); yellow (slightly electron rich region); and light blue (slightly electron deficient region), respectively. The potential increases in the order of red < orange < yellow < green < blue [50]. As shown in the MEP of the title molecule 5 (Figure 7), regions with negative potential are on the electronegative atoms (nitrogen atom of the pyrazole moiety and oxygen atom of the hydroxyl group that offer on its surface a potential of -30.073 and -27.842 Kcal/mol respectivelly). Positive region was found on the hydrogen atom of the imine group, offering a potential of 24.538 Kcal/mol on its surface, indicating that this site may most likely be involved in nucleophilic processes. From the MEP, it can be inferred that these compounds can be used as ligands in palladium or platinum complexes, which can be coordinated through the N-3 in compound **3** and N-18 in compound **5** and not by the azomethyne C=N moieties.

Insert Figure 7.

4.8. Global reactivity descriptor

Increased LUMO energy level and decreased HOMO energy level results in higher HOMO-LUMO gap. Higher HOMO-LUMO gap corresponds to higher kinetic stability, thus, lower chemical reactivity [45-47]. That is, a small interval between HOMO-LUMO implies low kinetic stability and high chemical reactivity, as it is energetically favorable to add electrons to a LUMO and to extract electrons from a HOMO. The HOMO-LUMO energy of the compound **3** is 4.15 eV and the HOMO-LUMO energy of the compound **5** is 3.92 eV, as shown in **Figure 8**, whereby it can be inferred that compound **3** has higher stability while compound **5** has higher reactivity. Among many others, the energy difference between HOMO and LUMO has been used to predict the activity and intramolecular charge transfer in organic molecules with conjugated π bonds [51-52].

Insert Figure 8.

The quantum chemical properties led us to know how to find the energy states of the molecules. Chemical bonds are a source of energy and the movement of molecules in the space is kinetic energy. The vibrations and rotations of molecules is another source of chemical energy along with the chemical reaction, which is a rearrangement of atoms.

Density functional theory has been successful in providing insights into the chemical reactivity and selectivity in terms of global parameters, like electronegativity, hardness, and softness [53].

The concept of hardness/softness is related to the reactivity of the molecules and it is a property that measures the extent of chemical reactivity to which the addition of a charge stabilizes the system. The chemical potential provides a global reactivity index and is related to charge transfer from a system of higher chemical potential to one of lower chemical potential. Electronegativity is the power to attract electrons and it is related directly to all above properties mentioned. All these properties are defined as follows [54-55]. The electrophilicity index is a measure of decrease in total energy during electron sharing [56].
The ionization potential (IP) and electron affinity (EA) can be calculated from the HOMO and the LUMO energies using Koopmans' approximation, where IP = - HOMO and EA = - LUMO: the chemical potential μ and χ are defined as [54]:

$$-\mu \approx \chi = \frac{IP + EA}{2}$$

The larger the HOMO-LUMO energy gap, the harder the molecule will be [57]. Chemical hardness can be calculated as follows:

$$\eta = \frac{IP - EA}{2}$$

Global softness is the inverse of global hardness [58]:

$$\sigma = \frac{1}{\eta}$$

Parr *et al*., [55] introduced the global electrophilicity index (ω), which measures the propensity of a species to accept electrons. It can be calculated by using the electronic chemical potential (μ) and chemical hardness (η):

$$\omega = \frac{\mu^2}{2\eta}$$

Molecules with a large HOMO-LUMO energy gap are called “hard” and those with a small HOMO-LUMO energy gap are called “soft”. Frontier orbitals (HOMO – LUMO) of the compounds **3** and **5** were calculated by using B3LYP/6-31G**. The hardness *vs* softness of the title compounds are compared in order to obtain a better knowledge of the effect of the substituents on their pyrazole rings. The HOMO-LUMO energy gap, electronegativity, electrophilicity index, and chemical hardness and softness values of compounds **3** and **5** are listed in **Table 7**.

Insert Table 7.

Compound **3** has 2.08 hardness, being harder than compound **5** (1.96), so it has a lower electronegativity, indicating that the molecule is relatively hard so it tends to undergo changes or reactions easily [54]. A molecule with a small frontier orbital gap is more polarizable and is generally associated with a high chemical reactivity, low kinetic stability and is also termed as a soft molecule [59]. Compound **5** with a smaller energy gap, with respect to compound **3**, is considered a soft molecule. The electrophilicity index (ω) is a measure of the energy stabilization that occurs when the system acquires an additional charge from the environment. Compound **3**, have a great chemical hardness, so its electrophilicity index will be low. As expected, 4-bromo phenyl moiety in **5** increases the electronegativity of this compound, contributing to lower hardness and higher electrophilicity index.

5. Conclusion

Two new pyrazolic Schiff-bases **3** and **5**, were synthesized and characterized by different spectroscopic and analytical techniques, such as FT-IR, ^{1}H NMR, ^{13}C NMR, DEPT 135, 2D NMR (HSQC, HMBC), UV-Vis, MS and single-crystal X-ray diffraction. The compound **3** crystallized in the space group I41/a, while, its analogous **5** crystallized in the space group $P2_1/c$. The obtained data via X-ray diffraction and computational calculations indicated a good correlation between experimental and theoretical data.

In order to predict the reactive sites for electrophilic and nucleophilic attacks in both molecules, MEP´s were calculated in the optimized geometries.

The reactivity descriptors showed that compound **5** is softer than compound **3**, showing that compound **5** tends to make changes or react more easily.

Acknowledgement

Total financial support from the Vice-Rectory of Research (Projects 789 y 920) from Universidad del Quindío (Armenia, Colombia) is gratefully acknowledged.

References

[1] A. Tewari, A. Mishra, Synthesis and anti-inflammatory activities of N4,N5-disubstituted-3-methyl- *H*-pyrazolo[3,4-c]pyridazines, Bioorg. Med. Chem. 9 (2001) 715-718.

[2] Y. Xia, Z. W. Dong, B. X. Zhao, X. Ge, N. Meng, D. S. Shin, J. Y. Miao, Synthesis and structure–activity relationships of novel 1-arylmethyl-3-aryl-1*H*-pyrazole-5-carbohydrazide derivatives as potential agents against A549 lung cancer cells, Bioorg. Med. Chem. 15 (2007) 6893–6899.

[3] V. Michon, C. Hervé du Penhoat, F. Tombret, J. Gillardin, F. Lepage, L. Berthon, Preparation, structural analysis and anticonvulsant activity of 3- and 5-aminopyrazole *N*-benzoyl derivatives, Eur. J. Med. Chem. 30 (1995) 147–155.

[4] R. Sridhar, P. Perumal, S. Etti, G. Shanmugam, M. Ponnuswamy, V. Prabavathy, N. Design, Synthesis and anti-microbial activity of 1*H*-pyrazole carboxylates, Bioorg. Med. Chem. 14 (2004) 6035-6040.

[5] W. Herrmann, R. Kratzer, H. Ding, W. Thiel, H. Glas, Methyltrioxorhenium/pyrazole—A highly efficient catalyst for the epoxidation of olefins , J. Organomet. Chem. 555 (1998) 293–295.

[6] J. L. Liao, Y. Chi, Z.T. Sie, C.H. Ku, .C.H. Chang, M. A Fox, P. J. Low, M.R. Tseng, G.H. Lee, Ir(III)-Based Phosphors with Bipyrazolate Ancillaries; Rational Design, Photophysics, and Applications in Organic Light-Emitting Diodes. Inorganic Chemistry, 54 (2015) 10811–10821.

[7] T. Ren, H. Cheng, J. Zhang, W. Li, J. Guo, L. Yang, Synthesis of benzimidazoles containing pyrazole group and quantum chemistry calculation of their spectroscopic properties and electronic structure, J. Fluoresc. 22 (2012) 201–212.

[8] H. Liu, F. X. Li, Y. Pi, D. Wang, Y. Hu, J. Zheng, Fluorescence quenching study of 2,6-*bis*(5-(4-methylphenyl)-1*H*-pyrazol-3-yl)pyridine with metal ions, Spectrochim. Acta A. 145 (2015) 588–593.

[9] D. Sek, M. Siwy, M. Grucela, G. Małecki, E. Nowak, G. Lewinska, J. Santera, K. Laba, M. Lapkowski, S. Kotowicz, E. Schab-Balcerzak, New anthracene-based Schiff bases: Theoretical and experimental investigations of photophysical and electrochemical properties, Spectrochim. Acta A. 175 (2017) 24-35.

[10] S. Gandhimathi, C. Balakrishnan, M. Theetharappan, M. Neelakantan, R. Venkataraman, Noncovalent interactions from electron density topology and solvent effects on spectral properties of Schiff bases, Spectrochim. Acta A. 175 (2017) 134–144.

[11] F. Cuenú, N. Patiño, J. Torres, R. Abonia, R. Toscano, J. Cobo, The new 3-(*tert*-butyl)-1-(2-nitrophenyl)-1*H*-pyrazol-5-amine: Experimental and computational studies, J. Mol. Struct. 1148 (2017) 557–567.

[12] R. Fuquen, F. Cuenú, J. Torres, G. De la Vega, E. Galarza, R. Abonia, A. Kennedy, Precense of π…π and C-H… π interactions in the new Schiff base 2- {(*E*)-[(3-*tert*-butyl-1-phenyl-1*H*-pyrazol-5-yl)imino]methyl}phenol: Experimental and DFT computational studies, J. Mol. Struct. 1150 (2017) 366–373.

[13] R. Abonia, E. Cortés, B. Insuasty, J. Quiroga, M. Nogueras, J. Cobo, Synthesis of novel 1, 2, 5-trisubstituted benzimidazoles as potential antitumor agents, Eur. J. Org. Chem. 46 (2011) 4062–4070.

[14] D. Zhu, Q. Xing, R. Cao, D. Zhao, W. Zhong, Synthesis and p38 Inhibitory Activity of Some Novel Substituted *N*,*N´*-Diarylurea Derivatives, Molecules 21 (2016) 677.

[15] M. Frisch, G. Trucks, H. Schlegel, G. Scuseria, M. Robb, J. Cheeseman, G. Scalmani, V. Barone, B. Mennucci, G.A. Petersson, H. Nakatsuji, M. Caricato, X. Li, H.P. Hratchian, A.F. Izmaylov, J. Bloino, G. Zheng, J.L. Sonnenberg, M. Hada, M. Ehara, K. Toyota, R. Fukuda, J. Hasegawa, M. Ishida, T. Nakajima, Y. Honda, O. Kitao, H. Nakai, T. Vreven, J.A. Montgomery Jr., J.E. Peralta, F. Ogliaro, M. Bearpark, J.J. Heyd, E. Brothers, K.N. Kudin, V.N. Staroverov, T. Keith, R. Kobayashi, J. Normand, K. Raghavachari, A. Rendell, J.C. Burant, S.S. Iyengar, J. Tomasi, M. Cossi, N. Rega, J.M. Millam, M. Klene, J.E. Knox, J.B. Cross, V. Bakken, C. Adamo, J. Jaramillo, R. Gomperts, R.E. Stratmann, O. Yazyev, A.J. Austin, R. Cammi, C. Pomelli, J.W. Ochterski, R.L. Martin, K. Morokuma, V.G. Zakrzewski, G.A. Voth, P. Salvador, J.J. Dannenberg, S. Dapprich, A.D. Daniels, O. Farkas, J.B. Foresman, J.V. Ortiz, J. Cioslowski, D.J. Fox, Gaussian 09, Revision D.01, Gaussian, Inc, Wallingford CT, 2013.

[16] (a) M. Jamroz, Vibrational Energy Distribution Analysis VEDA 4: scopes and limitations, Spectrochim. Acta. A 114 (2013) 220–230.

[17] M. O'Boyle, A. Tenderholt, K. Langner. Software News and Updates cclib: A Library for Package-Independent Computational Chemistry Algorithms, J. Comput. Chem. 29 (2008) 839–845.

[18] S. Murugavel, C.S. Jacob, P. Stephen, R. Subashini, H. Raveendranatha Reddy, D. AnanthaKrishnan, Synthesis, crystal structure investigation, spectroscopic characterizations and DFT computations on a novel 1-(2-chloro-4-phenylquinolin-3-yl)ethanone, J. Mol. Struct. 1122 (2016) 134–145.

[19]. N. J. Turro, Molecular structure as a blueprint for supramolecular structure chemistry in confined spaces, PNAS, 102 (2005) 10766-10770.

[20]. J. Bernstein, R. Davis, L. Shimoni, N. Chang. Angew, Patterns in Hydrogen Bonding: Functionality and Graph Set Analysis in Crystals, Chem Int Ed Engl. 34 (1995) 1555.

[21] A. Cruz, A. López, A. Ríos, F. Cuenú, C. Rozo, Experimental and theoretical studies on the structure and spectroscopic properties of (*E*)-1-(2-aminophenyl)-3-(pyridine-4-yl) prop-2-en-1-one, J. Mol. Struct. 1098 (2015) 216–228.

[22] K. Amareshwar Rai, D.K. Rai, Spectroscopic studies of some antidiabetic drugs, Spectrochim. Acta. A. 59 (2003) 1673–1680.

[23] S. Tanis, T. Parker, J. Colca, R. Fischer, R. Kletzein, Synthesis and Biological Activity of Metabolites of the Antidiabetic, Antihyperglycemic Agent Pioglitazone, J. Med. Chem. 39 (1996) 503–505.

[24] D. Michalska, D. Bienko, A. Abkowicz-Bienko, Z. Latajka, Density Functional, Hartree−Fock, and MP2 Studies on the Vibrational Spectrum of Phenol, J. Phys. Chem. 100 (1996) 17786–17790.

[25] G. Hartland, B. Henson, V. Venturo, P. Felker, Density Functional, Hartree−Fock, and MP2 Studies on the Vibrational Spectrum of Phenol, J. Phys. Chem. 96 (1992) 1164–1173.

[26] H. Freedman, Intramolecular H-Bonds. I. A Spectroscopic Study of the Hydrogen Bond between Hydroxyl and Nitrogen, J. Am. Chem. Soc. 83 (1961) 2900–2905.

[27] P. Binil, Y. Mary, H. Varghese, C. Panicker, M. Anoop, T. Manojkumar, Infrared and Raman spectroscopic analyses and theoretical computation of 4-butyl-1-(4-hydroxyphenyl)-2-phenyl-3,5- pyrazolidinedione, Spectrochim. Acta. A. 94 (2012) 101-109.

[28] F. Cuenú, J. Londono-Salazar, J. Torres, R. Abonia, R. D'Vries, Structural characterization and theoretical studies of a new Schiff base 4-(((3-(*tert*-Butyl)-(1-phenyl)pyrazol-5-yl) imino)methyl) phenol, J. Mol. Struct. 1152 (2018) 163–176.

[29] G. Varsanyi, Vibrational Spectra of Benzene Derivatives, first ed., Academic Press, New York, (1969).

[30] J. Coates, Encyclopedia of Analytical Chemistry, R. A. Meyers ed., John Wiley & Sons Ltd, Chichester, (2000) 10815–10837.

[31] S. Subashchandrabose, A. Krishnan, H. Saleem, R. Parameswari, N. Sundaraganesan, V. Thanikachalam, G. Manikandan, Vibrational spectroscopic study and NBO analysis on bis(4-amino-5-mercapto-1,2,4-triazol-3-yl) methane using DFT method, Spectrochim. Acta. A. 77 (2010) 877–884.

[32] A. Melha, K. Faruk, H. Bimetallic complexes of Schiff base bis-[4-hydroxycuomarin-3-yl]-^{1}N,^{5}N-thiocarbohydrazone as a potentially dibasic pentadentate ligand. Synthesis, spectral, and antimicrobial properties, J. Iran. Chem. Soc. 5 (2008) 122–134.

[33] Y. Mary, C. Panicker, M. Sapnakumari, B. Narayana, B. Sarojini, A. Al-Saadi, C. Van Alsenoy, J. Ahmad War, H. Fun, Infrared spectrum, structural and optical properties and molecular docking study of 3-(4-fluorophenyl)-5-phenyl-4,5-dihydro-1H-pyrazole-1-carbaldehyde, Spectrochim. Acta A. 138 (2015) 529–538.

[34] M. Ilic, E. Koglin, A. Pohlmeier, H. Narres, M. Schwuger, Adsorption and Polymerization of Aniline on Cu(II)-Montmorillonite: Vibrational Spectroscopy and ab Initio Calculation, Langmuir 16 (2000) 8946–8951.

[35] R. Bauernschmitt, R. Ahlrichs, Treatment of electronic excitations within the adiabatic approximation of time dependent density functional theory, Chem. Phys. Lett. 256 (1996) 454–464.

[36] L. Li, T. Li, Z. Wang, Z. Zhou, J. Wang, T. Sunet, Study on molecular structure, spectroscopic investigation (IR, Raman and NMR), vibrational assignments and HOMO–LUMO analysis of L-sodium folinate using DFT: A combined experimental and quantum chemical approach, Spectrochim. Acta A. 120 (2014) 106–118.

[37] H. P. Ebrahimi, J. Hadi, Z. Abdulnabi, Z. Bolandnazar, Spectroscopic, thermal analysis and DFT computational studies of salen-type Schiff base complexes, Spectrochim. Acta. A. 117 (2014) 485–492.

[38] K. Pihlaja, E. Kleinpeter, Carbon-13 Chemical Shifts in Structural and Stero Chemical Analysis, VCH Publishers, New York, (1994) 1127.

[39] P. Garratt, A. Katritzky, C. Rees, E.F.V. Scriven (Eds.), Comprehensive Heterocyclic Chemistry II, Elsevier Science, 4 (1996) 127–163.

[40] Ö. Tamer, N. Dege, D. Avcı, Y. Atalay, İ. İlhan, M. Çadır, Synthesis, structural and spectroscopic evaluations and nonlinear optical properties of 3,5-*bis*(4-methoxyphenyl)-4,5-dihydro-1*H*-pyrazole-1-carbothioic *O*-acid, Spectrochim. Acta. A. 137 (2015) 1387–1396.

[41] P. Tyagi, M. Tyagi, S. Agrawal, S. Chandra, H. Ojha, M. Pathak, Synthesis, characterization of 1,2,4-triazole Schiff base derived metal complexes: Induces cytotoxicity in HepG2, MCF-7 cell line, BSA binding fluorescence and DFT study, Spectrochim. Acta. A. 171 (2017) 246–257.

[42] V. Arjunan, R. Santhanam, T. Rani, H. Rosi, S. Mohan, Conformational, vibrational, NMR and DFT studies of -methylacetanilide, Spectrochim. Acta. A. 104 (2013) 182–196.

[43] H. Nazır, M. Yıldız, H. Yılmaz, M. Tahir, D. Ülkü, Intramolecular hydrogen bonding and tautomerism in Schiff bases. Structure of *N*-(2-pyridil)-2-oxo-1-naphthylidenemethylamine, J. Mol. Struct. 524 (2000) 241–250.

[44] Z. Demircioğlu, Ç. Kaştaş, O. Büyükgüngör, The spectroscopic (FT-IR, UV–vis), Fukui function, NLO, NBO, NPA and tautomerism effect analysis of (*E*)-2-[(2-hydroxy-6-methoxybenzylidene)amino]benzonitrile, Spectrochim. Acta A. 139 (2015) 539–548.

[45] J. Aihara, Reduced HOMO−LUMO Gap as an Index of Kinetic Stability for Polycyclic Aromatic Hydrocarbons, J. Phys. Chem. 103 (1999) 7487–7495.

[46] Y. Ruiz-Morales, HOMO−LUMO Gap as an Index of Molecular Size and Structure for Polycyclic Aromatic Hydrocarbons (PAHs) and Asphaltenes: A Theoretical Study, J. Phys. Chem. 106 (2002) 11283–11308.

[47] I. Fleming. J. Wiley, Frontier Orbitals and Organic Chemical Reactions, Sons LTD, London (1976). 879–880.

[48] J. Murray, K. Sen, Molecular Electrostatic Potentials, first ed., Elsevier, Amsterdam, (1996).

[49] J. Seminario, Recent Developments and Applications of Modern Density Functional Theory, first ed., Elsevier, 4 (1996) 800–806.

[50] T. Yesilkaynak, G. Binzet, F. Mehmet Emen, U. Florke, N. Kulcu, H. Arslan, Theoretical and experimental studies on N-(6-methylpyridin-2-yl-carbamothioyl)biphenyl-4-carboxamide, Eur. J. Org. Chem.1 (2010) 1.

[51] L. Padmaja, C. Ravikumar, D. Sajan, I. Hubert, V. Jayakumar, G. Pettit, O. Faurskov, Density functional study on the structural conformations and intramolecular charge transfer from the vibrational spectra of the anticancer drug combretastatin-A2, J. Raman. Spectrosc. 4 (2009) 419–428.

[52] C. Ravikumar, I.H Joe, V.S Jayakumar, Charge transfer interactions and nonlinear optical properties of push–pull chromophore benzaldehyde phenylhydrazone: A vibrational approach, Chem. Phys. Lett. 460 (2008) 552–558

[53] N. Sheela, S. Muthu, S. Sampathkrishnan, Molecular orbital studies (hardness, chemical potential and electrophilicity), vibrational investigation and theoretical NBO analysis of 4-40 -(1H-1,2,4-triazol-1-yl methylene) dibenzonitrile based on abinitio and DFT methods, Spectrochim. Acta. A. 120 (2014) 237–251.

[54] R. Parr, Density functional theory of atoms and molecules, Oxford University Press, Oxford, New York (1989) 101.

[55] R. Parr, L. Szentpaly, S. Liu, Electrophilicity Index., J. Am. Chem. Soc, 121 (1999) 1922– 1924.

[56] K. Carthigayan, S. Xavier, S. Periandy. HOMO–LUMO, UV, NLO, NMR and vibrational analysis of 3-methyl-1- phenylpyrazole using FT-IR, FT-RAMAN FT-NMR spectra and HF-DFT computational methods, Spectrochim. Acta. A. 142 (2015) 350–363.

[57] R. Pearson, Absolute electronegativity and absolute hardness of lewis acids and bases, J. Am. Chem. Soc. 107 (1985) 6801–6806.

[58] W. Yang, R. Parr, Hardness, softness, and the fukui function in the electronic theory of metals and catalysis, Proc. Natl. Acad. Sci. U. S. A. 82 (1985) 6723–6726.

[59] B. Powell, T. Baruah, N. Bernstein, K. Brake, R.H. McKenzie, P. Meredith, M.R. Pederson, A first-principles density-functional calculation of the electronic and vibrational structure of the key melanin monomers, J. Chem. Phys. 120 (2004) 8608–8615.

TABLES

Table 1. Crystallographic data and refinement parameters for compounds **3** and **5**

Compound	**3**	**5**
Emp. Formula	$C_{14}H_{17}N_3O$	$C_{20}H_{21}BrN_3O$
FW (g/mol)	243.30	398.30
Temp. (K)	123	298
λ (Å)	0.71073	0.71073
Crystal system	Tetragonal	Monoclinic
Space group	I41/a	P21/c
Unit cell	-	-
a (Å)	18.0282(5)	11.1456(11)
b (Å)	18.0282(5)	14.0544(8)
c (Å)	18.0795(9)	11.9729(11)
α (°)	90	90
β (°)	90	100.321(8)
γ (°)	90	90
Volume (Å^3)	5876.0(4)	1845.1(3)
Z	16	4
ρ calcd (mg/m^3)	1.100	1.387
Abs.Coeff (mm^{-1})	0.07	2.236
F(000)	2080	792
Θ range (°)	3.6 to 27	3.716 to 33.134
Reflections collected/ Unique [R(int)]	38985/3203[0.041]	49874/7020[0.0576]
Data/restraints/parameters	3203/0/174	7020/0/233
Gof on F^2	0.886	1.076
R1 [I>2σ(I)]	0.0517	0.0387
wR2[I>2σ(I)]	0.1468	0.0916

Table 2. Optimized and experimental geometries of compounds **3** and **5** in the ground state

Compound 3			**Compound 5**		
Parameters[a]	**Experimental (X-ray)**	**DFT/B3LYP 6-31G**(Δ[b])**	**Parameters[a]**	**Experimental (X-ray)**	**DFT/B3LYP 6-31G**(Δ[b])**
Bond Lengths (Å)					
N(5)-N(4)	1.352	1.347(6)	C(34)-O(44)	1.343	1.341(2)
C(13)-O(18)	1.349	1.338(11)	C(34)-C(22)	1.396	1.425(29)
C(13)-C(12)	1.391	1.404(13)	C(22)-C(35)	1.394	1.411(17)
C(12)-C(11)	1.377	1.388(11)	C(35)-C(36)	1.379	1.385(6)
()C(11)-C(10)	1.375	1.404(29)	C(36)-C(39)	1.373	1.404(31)
C(10)-C(9)	1.379	1.386(7)	C(39)-C(38)	1.342	1.388(46)
C(7)-N(6)	1.283	1.293(10)	C(22)-C(21)	1.444	1.444(0)
C(3)-N(4)	1.335	1.337(2)	N(21)-C(20)	1.275	1.298(23)
C(3)-C(2)	1.404	1.426(22)	N(5)-N(6)	1.374	1.359(15)
C(1)-N(5)	1.349	1.367(18)	C(2)-N(6)	1.322	1.336(14)
C(1)-C(19)	1.512	1.516(4)	C(2)-C(1)	1.414	1.411(3)
C1(9)-C(25)	1.507	1.547(40)	C(3)-N(5)	1.345	1.379(34)
C(19)-C(26)	1.550	1.547(3)	C(5)-N(24)	1.430	1.420(10)
C(19)-C(24)	1.514	1.539(25)	C(31)-C(24)	1.356	1.399(43)
H(23)-O(18)	0.876	0.999	C(31)-C(30)	1.388	1.394(6)
H(21)-N(5)	0.894	1.007	C(30)-C(28)	1.368	1.392(24)
			C(28)-C(26)	1.352	1.394(42)
			C(2)-C(7)	1.510	1.522(12)
			C(7)-C(10)	1.540	1.545(5)
			C(7)-C(8)	1.546	1.539(7)
			C(7)-C(9)	1.515	1.545(30)
Linear function formula		y=0.8333x+0.2482	Linear function formula		y=0.9081x+0.1441
R^2		0.9824	R^2		0.9382
Bond angles (°)					
O(18)-C(13)- C(8)	120.90	122.11	C(22)-C(34)-O(44)	122.42	122.15

C(12)-C(13)-O(18)	119.11	118.66	C(35)-C(22)-C(34)	117.50	118.81
C(11)-C(12)-C(13)	120.09	120.34	C(36)-C(35)-C(22)	121.68	121.37
C(10)-C(11)-C(12)	120.61	121.03	C(35)-C(36)-C(39)	118.68	119.10
C(11)-C(10)-C(9)	119.85	119.05	C(36)-C(39)-C(38)	122.23	121.05
C(2)-C(3)-N(4)	111.43	111.37	C(21)-C(22)-C(34)	122.11	121.60
C(1)-N(5)-N(4)	112.70	114.22	N(20)-C(21)-C(22)	121.54	122.43
C(19)-C(1)-N(5)	122.21	122.41	C(2)-N(6)-N(5)	105.49	105.93
C(25)-C(19)-C(1)	108.75	109.69	C(1)-C(2)-N(6)	110.81	110.96
C(26)-C(19)-C(1)	109.63	109.70	C(31)-C(24)-N(5)	120.45	121.51
C(24)-C(19)-C(1)	109.30	109.60	C(24)-C(31)-C(30)	120.21	119.97
H(23)-O(18)-C(13)	107.45	107.41	C(31)-C(30)-C(28)	118.83	119.53
H(21)-N(5)-N(4)	118.99	118.35	C(30)-C(28)-C(26)	120.89	120.94
			C(7)-C(2)-N(6)	120.63	119.78
			C(10)-C(7)-C(2)	110.16	109.06
			C(8)-C(7)-C(2)	109.11	110.37

[a] The atom numbering scheme of the molecular structure is given in **Figure 2.**

[b] Deviation from experimental and calculated data.

Compound	D-H…A	D-H	H…A	D…A	D…H…A
Compound 3	O1-H1H···N1	0.87(3)	1.78(3)	2.5734(18)	150.0(3)
	N3-H31···N2^{i}	0.89(2)	1.98(2)	2.8671(18)	171.3(18)
	C7-H7···O1^{ii}	1.01(2)	2.38(2)	3.3710(2)	167.2(16)
	C9-H9···O1^{ii}	0.95	2.39	3.3020(2)	161.0
Compound 5	O1-H1H···N1	0.85(3)	1.90(3)	2.6455(19)	145.0(3)
	C7-H7···N3^{iii}	1.01(2)	2.73(2)	3.5020(2)	133.4(15)

Table 3. Hydrogen-bond geometry (Å. ^{o}).

Code symmetry: (i) y+1/4.-x+3/4.-z+7/4; (ii) -y+1/4.+x-1/4.+z-1/4; (iii) x.-y+3/2.z+1/2.

Table 4. Assignments of vibrational wavelengths by VEDA 4 (cm^{-1}) for compounds **3** and **5.**

Compound 3				**Compound 5**			
Assignments	**Experimental**	**DFT/B3LYP**		**Assignments**	**Experimental**	**DFT/B3LYP**	
		Freq	%PED			Freq	%PED
νNH	3143	3530	100	-	-	-	-
νOH	-	3029	98	νOH	-	3161	98
$\nu C\text{-}H_{aromatic}$	3091	3089	99	$\nu C\text{-}H_{aromatic}$	3058	3081	84
$\nu C\text{-}H_{pyrazole}$	3085	3081	99	$\nu C\text{-}H_{pyrazole}$	3118	3150	99
$\nu_{as}CH_3$	2964	3003	98	$\nu_{as}CH_3$	2958	2983	99
$\nu_{s}CH_3$	2861	2925	98	$\nu_{s}CH_3$	2861	2963	97
νC=N	1614	1611	73	νC=N	1604	1598	17
$\nu C\text{-}C_{aromatic}$	1571	1550	44	$\nu C\text{-}C_{aromatic}$	1567	1540	57
δCH_3	1363	1360	63	δCH_3	1498	1458	69
νC-OH	1288	1291	32	δ H-O-C	1398	1392	34
δH-O-C	1213	1222	27	νC-OH	1282	1283	30

ν. stretching; δ. bending; s. symmetric; as. asymmetric. Potential Energy Distribution (PED).

Table 5. NMR theoretical shifts (δTheo.) and experimental (δExp.) for compound **3**, tautomer of compound **3** and compound **5.**

Compound 3			**Compound 5**		
Atom[a]	**Exp.**	**DFT**	**Atom[a]**	**Exp.**	**DFT**
H-26	1.31	1.30	**H-11**	1.34	1.37
H-27	1.31	1.36	**H-12**	1.34	1.30
H-28	1.31	1.36	**H-13**	1.34	1.32
H-29	1.31	1.45	**H-14**	1.34	1.33
H-30	1.31	1.45	**H-15**	1.34	1.37
H-31	1.31	1.62	**H-16**	1.34	1.68
H-32	1.31	1.62	**H-17**	1.34	1.68
H-33	1.31	1.75	**H-18**	1.34	1.89
H-34	1.31	1.75	**H-19**	1.34	1.96
H-20	6.33	6.66	**H-4**	6.70	6.69
H-17	6.95	7.07	**H-40**	6.95	7.08
H-15	6.97	7.18	**H-41**	7.00	7.24
H-16	7.40	7.63	**H-42**	7.44	7.64
H-14	7.61	7.64	**H-32**	7.62	7.68
H-22	9.07	8.94	**H-29**	7.62	7.72
H-21	12.61	9.42	**H-37**	7.70	7.73
H-23	13.23	13.45	**H-33**	7.73	7.83
-	-	-	**H-27**	7.73	8.06
-	-	-	**H-23**	9.12	8.90
-	-	-	**H-45**	11.61	12.45
Linear function formula	y=0.9014x+0.4573 R^2=0.9983		Linear function formula	y=1.0042x+0.1617 R^2=0.9946	
C-24	30.34	18.81	**C-8**	30.61	18.91
C-25	30.34	21.21	**C-10**	30.61	22.19
C-26	30.34	21.21	**C-9**	30.61	22.37
C-19	31.30	24.65	**C-7**	32.74	26.66
C-2	92.21	77.60	**C-1**	92.01	80.59
C-12	117.03	102.50	**C-38**	117.15	102.68
C-10	119.63	104.06	**C-36**	120.13	104.91
C-8	119.77	106.29	**C-22**	120.18	106.18
C-9	132.73	119.34	**C-28**	120.32	124.88
C-11	133.34	118.66	**C-25**	126.46	110.15
C-1	154.69	139.54	**C-31**	126.46	111.05
C-3	156.02	141.72	**C-35**	132.00	120.58
C-13	160.60	147.01	**C-26**	132.38	117.28
C-7	162.43	145.80	**C-30**	132.38	118.34
-	-	-	**C-39**	134.46	120.26
-	-	-	**C-24**	138.56	125.82
-	-	-	**C-3**	148.96	134.17
-	-	-	**C-34**	160.07	147.00
-	-	-	**C-2**	162.49	148.45

-	-	-	**C-21**	162.95	147.73
Linear function formula	y=0.9535x–8.1405 R^2=0.9991			y=0.9554x-7.0467 R^2=0.9900	

[a] The atom numbering scheme of the molecular structure is given in **Figure 2.**

Table 6. Experimental and theoretical electronic absorption wavelengths and important contributions for compounds **3** and **5.**

Compound 3					**Compound 5**				
Exp.	**DFT/B3LYP**				**Exp.**	**DFT/B3LYP**			
λ	**λ**	**E**	***f***	**Important contributions**	**λ**	**λ**	**E**	***f***	**Important contributions**
338	335	3.699	0.480	H→L (92%) H-1→L (6%)	360	364	3.399	0.496	H→L (96%) H-2→L (2%)
					325	315	3.928	0.215	H-2→L (92%) H→L (2%)
293	291	4.260	0.487	H-1→L (87%) H-2→L (3%) H→L (6%) H→L+1 (4%)					
					279	276	4.482	0.074	H-6→L (13%) H-4→L (10%) H-3→L (40%) H→L+1 (16%) H-8→L (7%) H-5→L (8%)
231	222	5.574	0.098	H-4→L (31%) H→L+1 (48%) H-1→L+1 (4%) H-1→L+2 (4%) H-1→L+3 (7%)	236	245	5.057	0.394	H-6→L (10%) H-5→L (19%) H-1→L+1 (52%) H-8→L (4%) H→L+1 (3%) H→L+3 (5%)
216	203	6.095	0.225	H-1→L+1 (49%) H→L+3 (39%) H-8→L (2%) H→L+1 (5%)	205	207	5.989	0.183	H-4→L+1 (14%) H-2→L+3 (26%) H→L+5 (42%) H-5→L+2 (2%) H-4→L+2 (5%)
193	180	6.873	0.255	H-8→L (24%) H-2→L+2 (58%)	195	185	6.702	0.169	H-12→L (17%) H-8→L+2 (12%)

			H-3→L+2 (16%) H-14→L (7%) H-13→L (2%) H-11→L (4%) H-9→L+1 (3%) H-4→L+2 (8%) H-2→L+5 (3%) H-1→L+5 (5%) H-1→L+6 (4%) H→L+6 (5%)
		H-4→L+1 (2%) H-1→L+2 (7%)	

λ: wavelengths (nm); *f*: oscillator strength; E: excitation energy (eV).

Table 7. HOMO - LUMO energies and calculated global chemical parameters of compounds **3** and **5** calculated via B3LYP/6-31G ** method.

Parameters	**Compound 3**	**Compound 5**
$\mathbf{E_{HOMO}}$	-6.24	-6.27
$\mathbf{E_{LUMO}}$	-2.08	-2.35
ΔE	4.15	3.92
Electronegativity (χ)	4.16	4.31
Chemical hardness (η)	2.08	1.96
Global softness (σ)	0.48	0.51
electrophilicity index (ω)	4.16	4.74

FIGURES

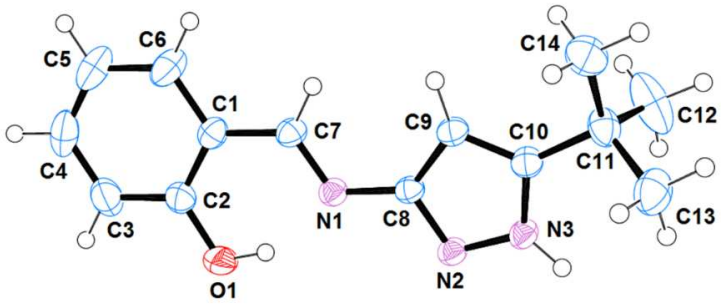

Compound 3

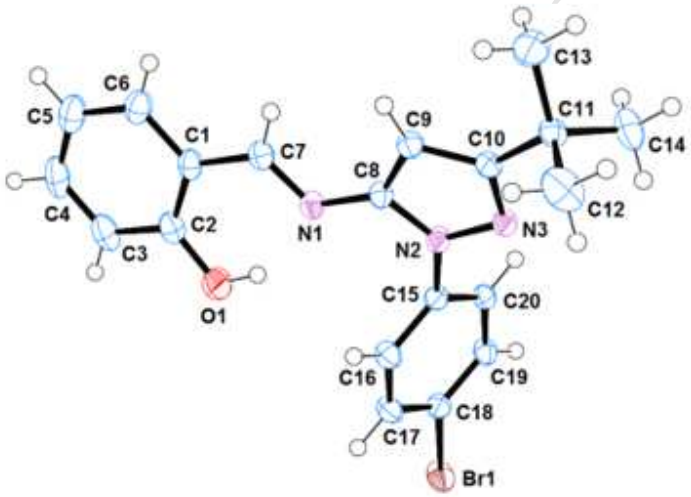

Compound 5

Figure 1. Molecular structure of compounds **3** and **5** obtained by X-ray diffraction.

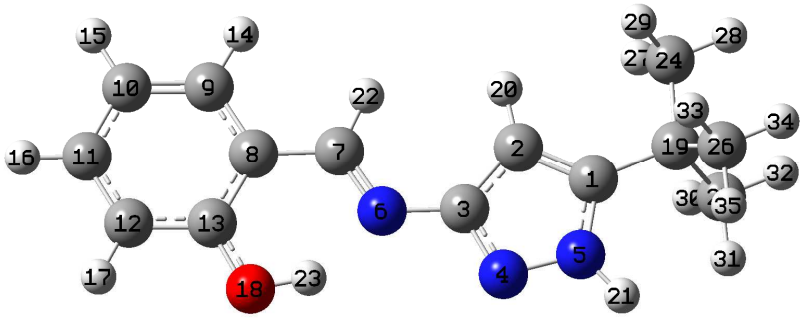

Compound 3

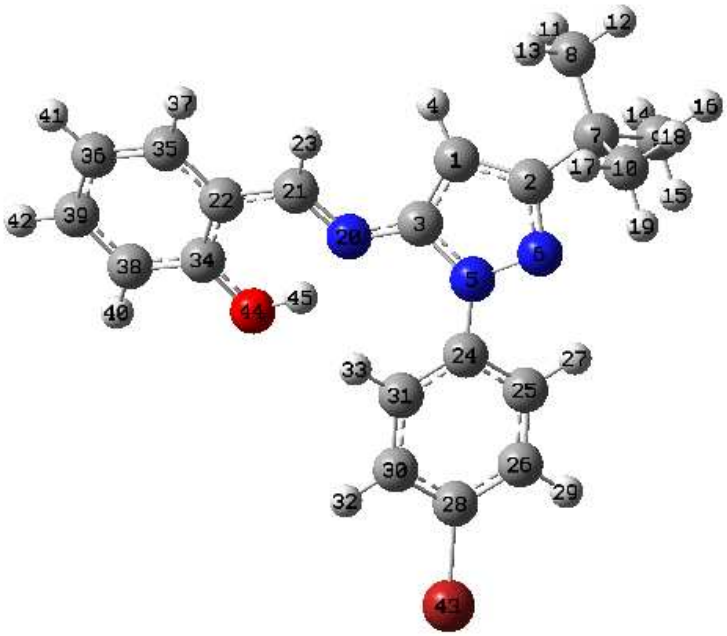

Compound 5

Figure 2. DFT-B3LYP optimized structure and numbering of atoms for compounds **3** and **5**.

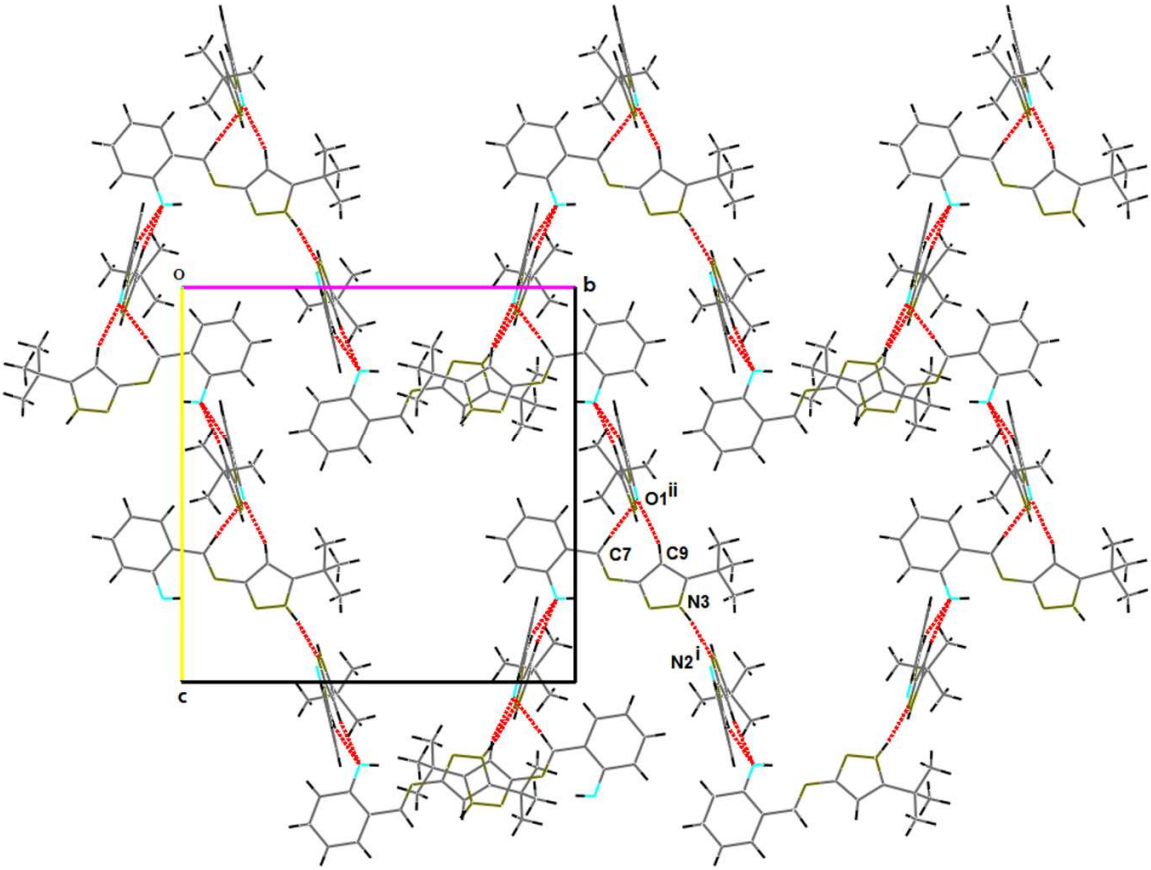

Figure 3. Partial packing diagram of compound **3** showing the two dimensional sheet network of molecules in the bc plane. The formation of which is governed by the occurrence of hydrogen bonds, forming edge-fused R^{15}_{14} (81) rings parallel to (100). Hydrogen bonds are predicted with dashed lines.

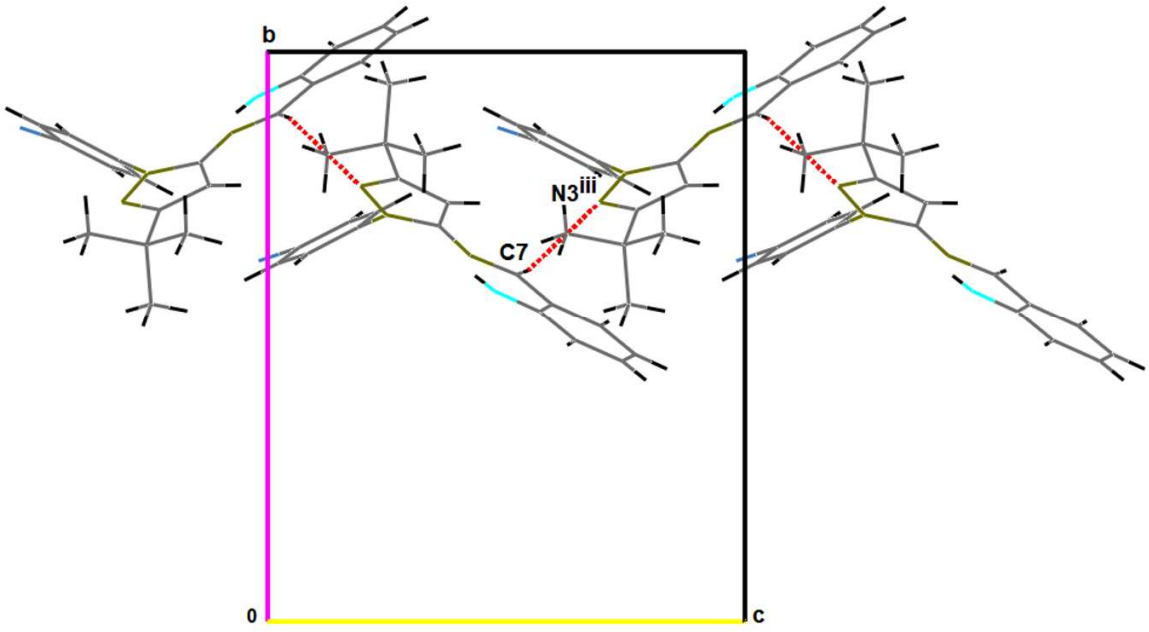

Figure 4. Partial packing diagram of compound **5** showing the two dimensional sheet network of molecules in the bc plane. Los enlaces de hidrógeno promueven la formación de cadenas de moléculas a lo largo de c. Hydrogen bonds are predicted with dashed lines.

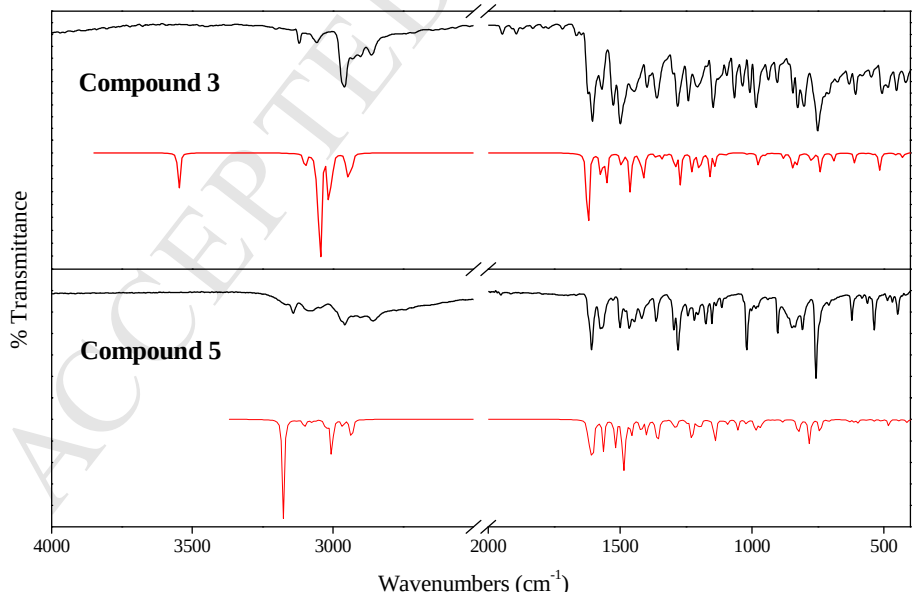

Figure 5. Experimental and calculated IR spectra of compounds **3** and **5**. The red line shows the theoretical spectra DFT/B3LYP and the black line shows the experimental spectra.

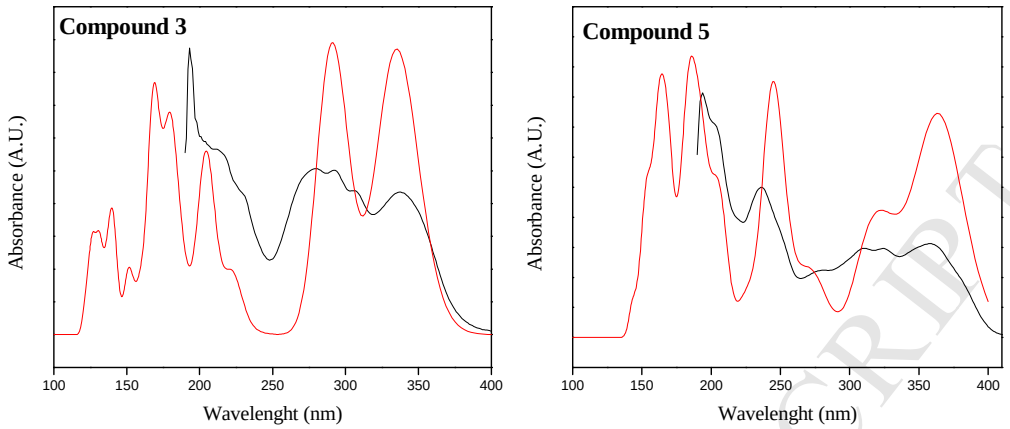

Figure 6. Comparison of experimental (black line) and theoretical (red line) UV-vis spectra for compounds **3** and **5**.

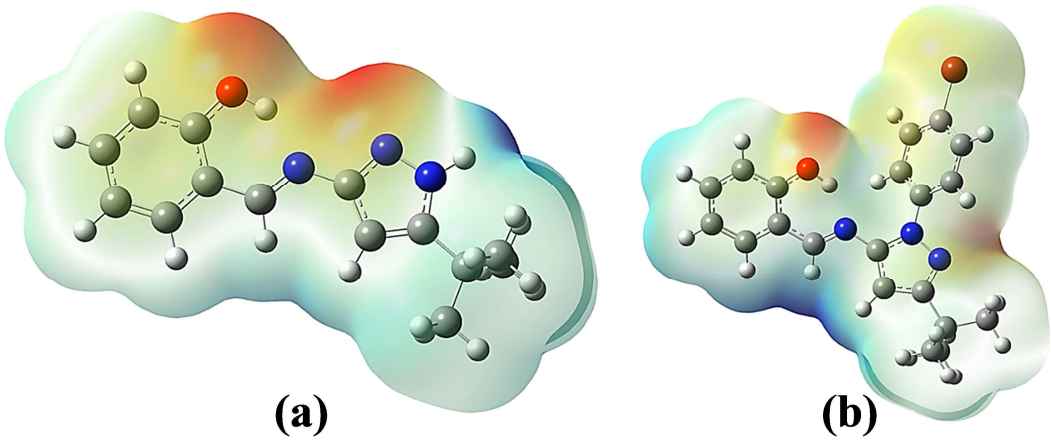

Figure 7. Electrostatic potential surface for compounds **(a)** compound **3** and **(b)** compound **5**, DFT/B3LYP level.

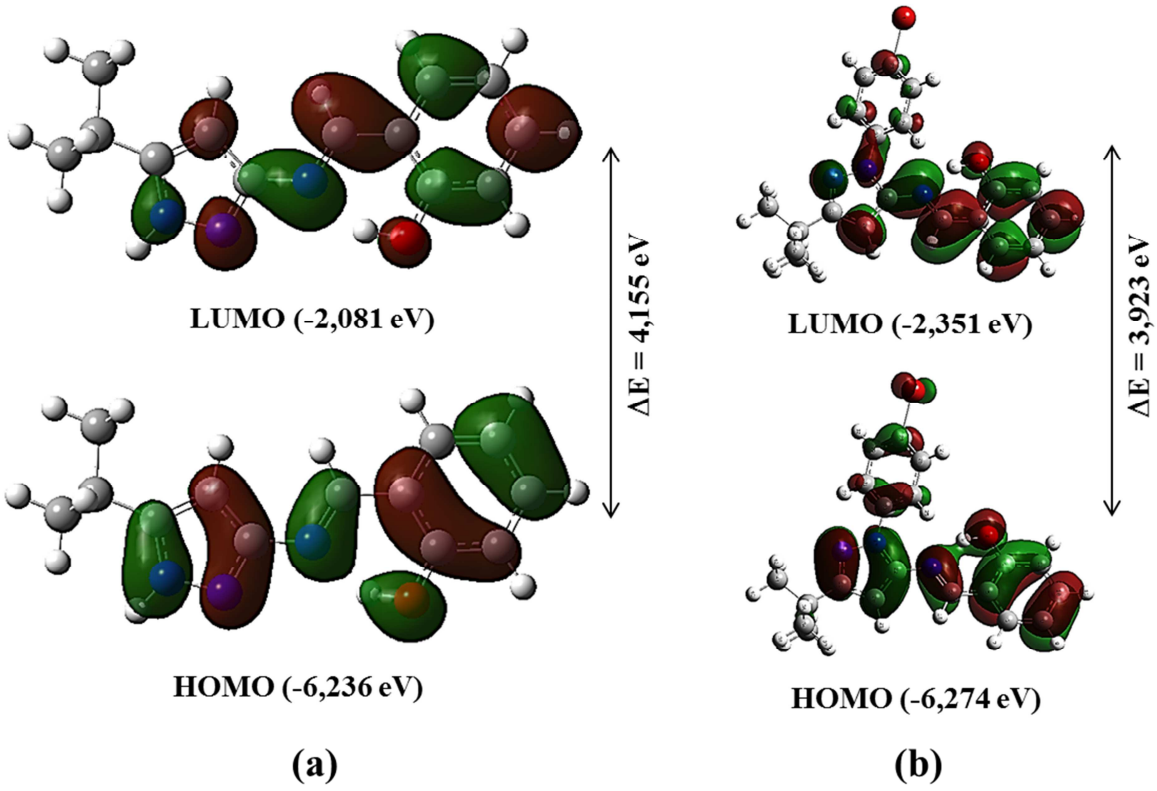

Figure 8. The HOMOs and LUMOs surfaces and energy values for: **(a)** compound **3** and **(b)** compound **5**.

SCHEMES

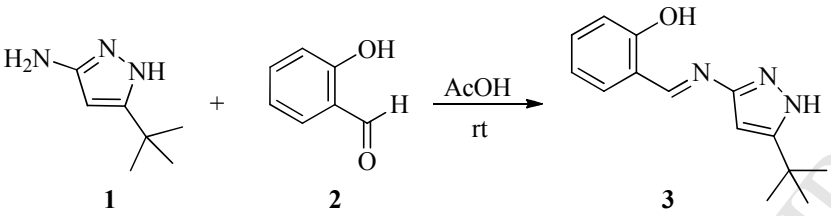

1 **2** **3**

Scheme 1. Synthesis of the compound **3**

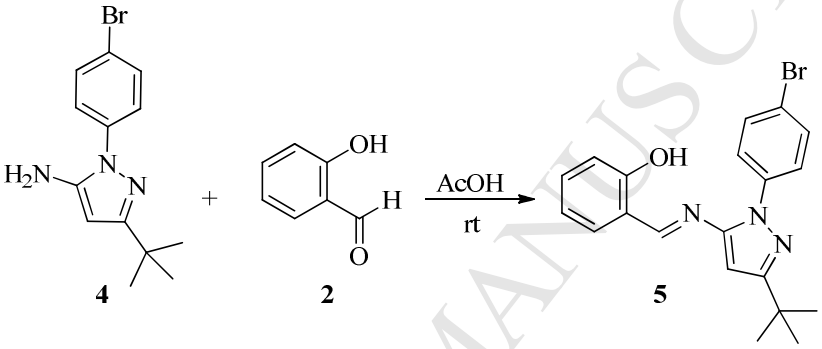

4 **2** **5**

Scheme 2. Synthesis of the compound **5**

HIGHLIGHTS

- Two novel molecules were synthesized.
- Chemical calculations of the obtained compounds were performed with the method DFT.
- MEP and NBO analysis of the new molecules were studied.
- The DFT theoretical results were compared with the experimental results.